DR-2789

UCRL-52981

Large-acceptance-angle gridded analyzers in an axial magnetic field

A. W. Molvik

June 1, 1981

UCRL-52981
Distribution Category: UC-20, 20f

Large-acceptance-angle gridded analyzers in an axial magnetic field

A. W. Molvik

Manuscript date: June 1, 1981

LAWRENCE LIVERMORE LABORATORY
University of California • Livermore, California • 94550

Available from: National Technical Information Service • U.S. Department of Commerce
5285 Port Royal Road • Springfield, VA 22161 • $6.00 per copy • (Microfiche $3.50)

CONTENTS

Large-acceptance-angle gridded analyzers in an axial magnetic field

ABSTRACT

Electrostatic retarding-potential gridded analyzers have been used to measure the current and the axial energy distributions of ions escaping along magnetic field lines in the 2XIIB magnetic mirror fusion experiment at Lawrence Livermore National Laboratory (LLNL). Three analyzers are discussed: a large scanning analyzer with a movable entrance aperture that can measure ion or electron losses from a different segment of the plasma diameter on each shot, a smaller analyzer that mounts in 5-cm-diam ports, and a multicollector analyzer that can continuously measure losses from the entire plasma diameter. The scanning and the 5-cm analyzers both operated successfully. The multicollector analyzer was designed, but not built. Careful electromagnetic shielding and grounding were necessary in order to reduce spurious signals. Accurate ion current measurements require grids that transmit ion trajectories at angles of 23° from axis, entrance grids that attenuate the plasma flow and isolate it from the analyzer grid potentials, several techniques to suppress secondary and primary electrons, and consideration of the space-charge limits as well as techniques to increase these limits. Accurate measurements of ion energy require, in addition, confining large-angle ion orbits within the analyzer (this requirement is relaxed on the Tandem Mirror Experiment (TMX), where the end-loss ions are more collimated), limiting the sweep rate of the ion repeller grid, and aligning the analyzer so that it is normal to the magnetic field lines. The analyzers measure the axial energy, which in these experiments is much greater than the transverse energy. Several pitfalls and their cures are identified in the design, construction, and operation of these analyzers.

INTRODUCTION

Electrostatic gridded analyzers were used to measure the current and energy distribution of unconfined ions in the 2XIIB magnetic-mirror plasma

confinement experiment.[1] As shown in Fig. 1, these unconfined ions escaped along the magnetic field to the end walls; there, the analyzers measured the ion current and/or the distribution of ion energies. Ion energies parallel to the axial magnetic field were measured.

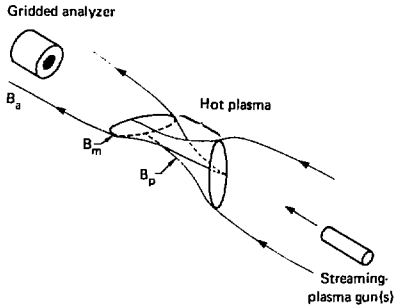

FIG. 1. Gridded analyzers measure the current and the energy distribution of end-loss ions, those lost from the 2XIIB magnetic-mirror-confined hot plasma as well as those from the streaming-plasma gun that are transmitted through the hot plasma. The ions flow along the magnetic field that increases from B_p = 7 kG at the hot plasma to B_m = 13 kG at the magnetic mirrors, then decreases to B_a = 2 kG at the analyzer.

Measurements of plasma loss currents are made in order to determine particle and energy containment of a hot plasma and for comparison with theoretical predictions of the unconfined ion current required for stabilization of loss-cone instabilities.[2] Measurements of the energy distribution of unconfined ions yield information on the plasma potential, rate of ionization of cold gas, and ion energy diffusion. [Note: these analyzers are now being used on the Tandem Mirror Experiment (TMX),[3] where they can determine the plasma potential and the central-cell ion temperature in addition to the loss current.]

Analyzers having several unique features were required to make such measurements on the 2XIIB experiment:

- The acceptance angle required to collect and analyze the energy of the ions at any angle within the loss cone exceeded 23°. (The loss cone is the boundary between magnetically trapped and unconfined ions.) The large acceptance angle is possible with these retarding-potential gridded analyzers because an axial magnetic field confines the ions to orbits smaller than the analyzer radius. The large acceptance angle contrasts with the low acceptance angle required by magnetic-field-free gridded analyzers.[4] The latter type of design is satisfactory for the TMX where the acceptance angle need be only

3.4°. In this report, we discuss the design of wide acceptance angle analyzers, as well as how the design problems are eased with collimated ions.

- A large dynamic range is required to measure incident current densities from 10^{-3} to 10^{1} A/cm^2 in a noisy environment within 100 μs after a streaming-plasma gun has fired directly into the analyzer. The large dynamic range is achieved by providing careful electromagnetic shielding and grounding, by attenuating the incident plasma with low-transmission entrance grids, and, when necessary, by increasing the ion space-charge-limited current by biasing the collector negatively. The current is also increased from that achieved with a single-hole entrance aperture,[4,5] without increasing the current density, by using a large entrance aperture (3 to 5 cm^2) covered with a grid.
- Secondary electrons are suppressed by the axial magnetic field and by the arrangement of grids, as well as by conventional electron-suppressor grids.
- Accurate measurements of the axial energy distribution of the ions are achieved by ensuring that all ion trajectories intercept the collector, by minimizing the time of flight of the ions from the ion repeller grid to the collector with swept bias analyzers, by using double grids,[6] and by minimizing the mixing of axial and transverse energy.

This report is divided into three major sections followed by a short critique of analyzer designs. In Sec. I, we describe the designs of three analyzers: a large scanning analyzer with a movable entrance aperture that can measure ion or electron losses from a different segment of the plasma diameter on each shot, a smaller analyzer that mounts in 5-cm-diam ports, and a multi-collector analyzer that can continuously measure losses from the entire plasma diameter. Also, we discuss some general mechanical and electrical features. In Sec. II, we discuss those details of the analyzer design that are necessary for accurate measurements of ion current but that are not sufficient for measuring energy. These details include grid transmission at angles up to 23° off axis, entrance-grid functions and designs, techniques for electron suppression, space-charge limits, electron current and energy measurements, and the mapping of currents along magnetic field lines. In Sec. III, we discuss additional design details that must be considered in order for the analyzers to obtain accurate measurements of the ion energy distribution function. These include the following: the confinement of large-angle ion trajectories within the analyzer (as well as less stringent design criteria

that are appropriate for collimated ions) methods for minimizing mixing of axial and transverse energy, and a criterion for choosing a sweep rate for the ion-repeller that does not limit resolution of ion energies. Section III concludes with example measurements of ion energy distribution, taken with the scanning analyzer. The 5-cm analyzer performed in a similar fashion.

I. ANALYZER DESCRIPTION

Two gridded analyzers were used on the 2XIIB magnetic mirror experiment and a third was designed but not built. One of those used on 2XIIB, a scanning analyzer (Fig. 2), was mounted inside the vacuum chamber. It used grids of up to 25-cm open diameter and included a sliding 1- by 5-cm entrance aperture to allow currents to be measured at various plasma radii. The aperture moved ±6 cm, scanning the minor diameter of the plasma from shot to shot. An outer case and an entrance grid at machine ground shielded the inner case at diagnostics room ground. This scanning analyzer measured ion energy distributions up to 3 keV, at which level it was limited by electrostatic forces on the grids.

The second analyzer, the 5-cm-diam analyzer (Fig. 3), was used on both 2XIIB and TMX. It was designed for installation outside the vacuum chamber in the 5-cm-diam ports usually used for streaming-plasma guns. Although it was primarily used for measuring the current density of the ions, it could also determine ion energy distributions up to 0.6 keV in a 2-kG magnetic field in 2XIIB. Beyond 0.6 keV, large ion orbits can intercept the entrance tube or miss the collector, as will be discussed in Sec. III.A. Such an energy limit does not exist with the more collimated ions on TMX, if one accepts slightly reduced energy resolution (Sec. III.B). Electromagnetic shielding, discussed in Sec. I.B, was particularly important for this analyzer because it could be installed between streaming-plasma guns that drew a current of typically 3 kA with open circuit voltages of approximately 2 kV. Polyethylene insulation around the analyzer separated it from adjacent plasma guns by providing a several kilovolt isolation between grounds. Electrical connections through the vacuum wall were made with vacuum-brazed coaxial connectors.

A third analyzer, which was designed but not built, uses a vertical array of eight collectors behind a vertical entrance slit to simultaneously measure the ion current and energy distributions at different plasma radii (Fig. 4). This multicollector analyzer provides data simultaneously at eight radii, is

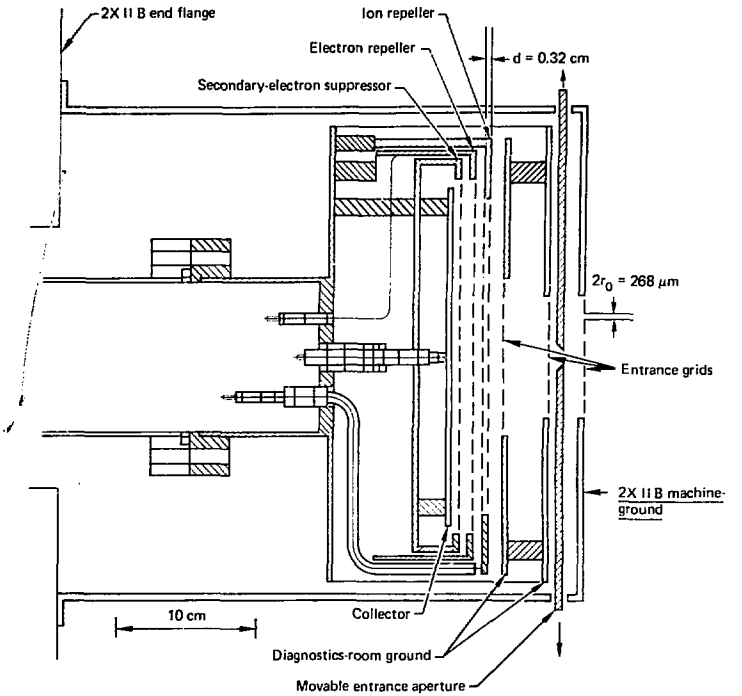

FIG. 2. The scanning end-loss analyzer was mounted inside the 2XIIB vacuum chamber and was enclosed by two separately grounded shields. An outer shield, grounded to 2XIIB, supported an entrance grid and a movable entrance aperture for scanning the spatial profile of end losses. An inner shield, grounded at the diagnostics room, enclosed ion- and electron-repeller grids, the secondary electron suppressor grid, the collector, and the cables from the analyzer to the diagnostics room. The grounds were connected at the analyzer with a low-inductance resistor of about 100 Ω. The analyzer and inner shield were mechanically isolated from the 2XIIB end flange with welded bellows (not shown) to protect the fragile grids and insulators from mechanical shock. Plasma was incident from the right. Flat grids, indicated by dashed lines, are mounted on rings that are normal to the axial magnetic field. The rings are supported on ceramic standoff-insulators and are connected through vacuum feedthroughs to bias power supplies. The apertures of different grids, including the double grids, are not aligned, but are randomly oriented relative to each other.

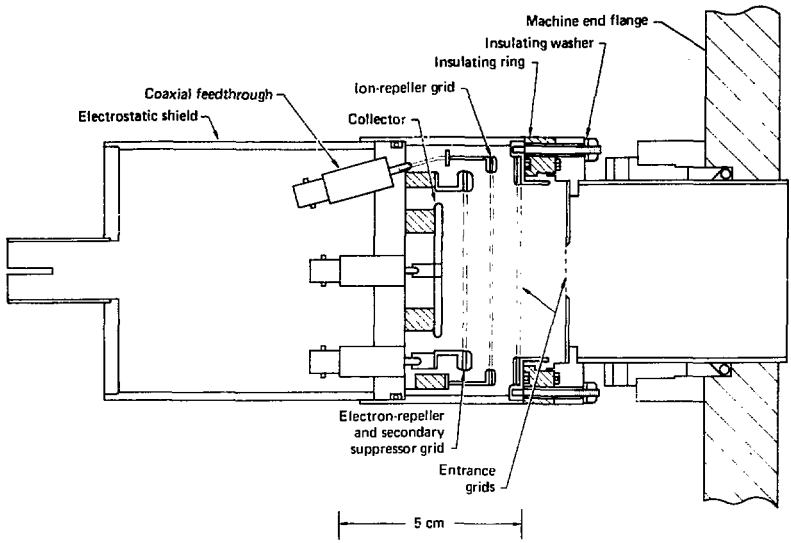

FIG. 3. The 5-cm analyzer was mounted in a 5-cm-diam port of the streaming-plasma guns on both 2XIIB and TMX. The entrance tube and grid at machine ground were electrically isolated from the rest of the analyzer, which was enclosed by a grid and vacuum wall at diagnostic-room ground. An electrostatic shield enclosed cable connectors and was connected to the conduit to the diagnostics room. The hermetically sealed coaxial connectors were vacuum brazed into the vacuum wall. To withstand mechanical shock, the structure was ruggedly built.

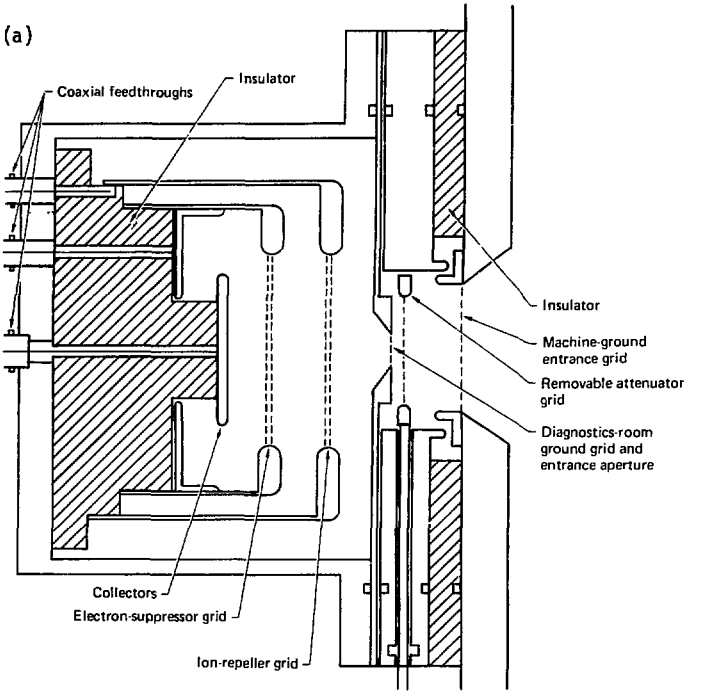

FIG. 4. The multicollector analyzer was designed to measure ion currents or energy distributions simultaneously at eight plasma radii. The sensitivity of the analyzer could be changed by inserting a low-transmission grid connected to a shaft through the vacuum wall. Grid supports were radiused to hold 10 kV between grids, and a modular design allowed convenient disassembly. The design was simplified as follows from the scanning analyzer: multiple collectors replaced a movable entrance aperture, external mounting provided easier access to the analyzer at the expense of slightly reduced energy resolution due to the less uniform magnetic field, and rugged insulators and lightweight grid supports withstand mechanical shock without requiring isolation bellows. An electrostatic shield (not shown) would enclose the cables as with the 5-cm analyzer. Unlike the cylindrical scanning and the 5-cm analyzers, the multicollector analyzer is rectangular. We show the end view in (a) and the side view, exhibiting the multiple collectors, in (b). This analyzer has not been built.

(b)

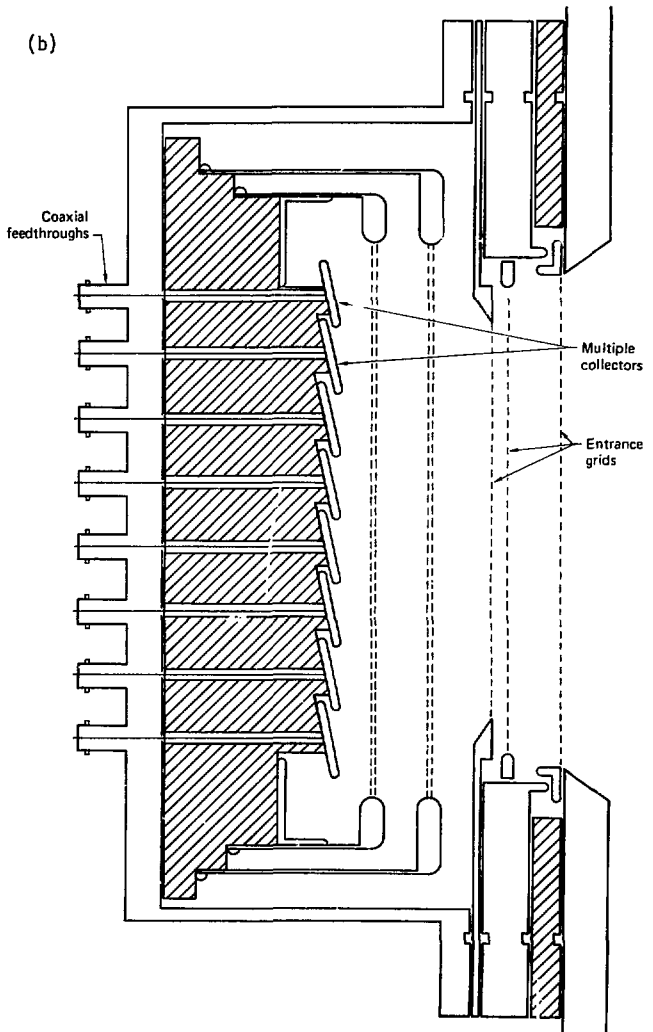
Coaxial
feedthroughs
Multiple
collectors
Entrance
grids

simpler mechanically than the scanning analyzer with its movable aperture, and is more easily disassembled for maintenance than the scanning analyzer. Being mounted outside the vacuum wall like the 5-cm-diam analyzer, it is more accessible for maintenance. This location entails some sacrifices in energy resolution, as will be discussed in Sec. III.D.

A. MECHANICAL DESIGN

The proper choice of grids is one of the more critical analyzer design problems. The properties of grids used in the scanning analyzer are listed in Table 1. Similar grids are used in the 5-cm-diam analyzer. Achieving a wide angular acceptance requires using grids that are thin, relative to the hole diameters, as will be discussed in Sec. II.A. Since the hole diameters must also be small, we selected nickel electroplated grids as thin as 5 μm. Mounting these fragile grids on rings of an open diameter up to 25 cm requires care to avoid wrinkles and to keep the grids taut. J. H. Williams developed the technique of first attaching the grid to a larger frame with light springs to hold it taut and flat, then laying it on the stainless-steel mounting ring and spot welding every, or nearly every, grid wire to the ring.

These grids remained taut if handled carefully and not overheated. Results of tests in an oven indicated that the electroplated nickel grids had little elasticity. When heated to 50°C, the stainless-steel mount expanded slightly more than the nickel grid; the grid stretched inelastically and did not remain taut as it cooled. Similar grid heating could have occurred in the analyzers in 2XIIB or TMX, where, to provide better pumping, all walls were coated with titanium evaporated from hot wires. To prevent nearby hot-titanium wires from overheating the grids, the housing (at diagnostics-room ground) of the scanning analyzer was therefore water cooled. The 5-cm analyzer, mounted outside the vacuum wall of 2XIIB or TMX, was sufficiently well shielded from heat sources that it did not require water cooling. Similarly, the multicollector analyzer would not be expected to require cooling.

To avoid distortion of electrostatic potential contours due to surface charges on insulators, all three analyzers are designed to hide the insulator from the charged particles being analyzed. All surfaces within line of sight of the ions or electrons are metal.

TABLE 1. Grid characteristics for scanning analyzer.
See Fig. 2 for the definitions of r_0 and d.

Grid function		Hole diameter, $2r_0$, (μm)	Maximum ion density, n_i (cm^{-3})	Grid thickness (μm)	Cutoff angle (degrees)	Transmission, T 0°	Transmission, T 16°	Grid separation, d (cm)
Entrance at machine ground	G1	268	not applicable	180	68	0.125	0.124	6.24
Entrance at diagnostics ground	G2	19	2.7×10^{12}	100	40	0.023	0.018	0.32
	G3	39	6.4×10^{11}	5	83	0.60	0.55	1.03
Ion repeller	I1	216	2.1×10^{10}	5	89	0.75	0.74	0.32
	I2	216	2.1×10^{10}	5	89	0.75	0.74	0.64
Electron repeller	E1	216	2.1×10^{10}	5	89	0.75	0.74	0.36
Electron suppressor	E2	216	2.1×10^{10}	5	89	0.75	0.74	0.36

Deposits on grid surfaces can become charged to voltages different from those applied, thereby distorting measurements of energy.[4-6] Since we cannot bake these analyzers to remove surface deposits, we minimize them by handling grids only with gloved hands, and by degreasing the other analyzer parts. This has been satisfactory at the several-hundred-eV energies encountered on 2XIIB and TMX.

Mechanical shock waves transmitted along the vacuum vessel from 0.6-ms risetime, pulsed magnet coils on 2XIIB were capable of breaking insulators used to support grids. The scanning analyzer, of rather fragile design, was mechanically isolated via a welded bellows (not shown in Fig. 2) and was supported independently of the vacuum vessel. This support system functioned well, but was awkward to handle and install. The 5-cm analyzer, on the other hand, incorporated a more rugged, yet lightweight, structure that could survive the shock waves and was therefore mounted directly to the vacuum vessel. The multicollector analyzer structure was also designed to withstand mechanical shock.

The maximum voltage between grids is determined not so much by voltage breakdown as by the allowable bowing of grids from electrostatic forces. Grid bias voltages are limited to 3 kV in the scanning analyzer, where 25-cm-diam, 5-μm-thick grids are separated by 0.6 cm. Higher bias voltages can be obtained either by increasing the grid strength or by increasing the grid-to-grid separation to decrease the electrostatic forces (subject to the other constraints to be discussed in Secs. II and III). Both techniques, along with more careful radiusing of grid holders, allow the 5-cm (and presumably the multicollector) analyzer to hold voltages greater than 10 kV.

B. ELECTRICAL DESIGN

Careful shielding and grounding are essential to an analyzer's having a large dynamic range in a high-electromagnetic-noise environment. Electromagnetic noise in 2XIIB originated from switching of 3000-A streaming-plasma guns, from sparkdown of multimegawatt neutral-beam injectors, and from switching of 1-MA turn, 0.6-ms risetime electromagnets. The electromagnets can also cause large ground-loop currents. The collector and repeller grids of all three analyzers described in this report were shielded by being surrounded by a

metal case that was closed to electromagnetic radiation at the entrance aperture by multiple, grounded entrance grids (Figs. 2 through 4) and that formed an extension of the 50-m-long conduit that enclosed all the coaxial cables, from the analyzer to the diagnostics room (Fig. 5). The coaxial cables carried the collector current and connected ion- and electron-repeller grids to the

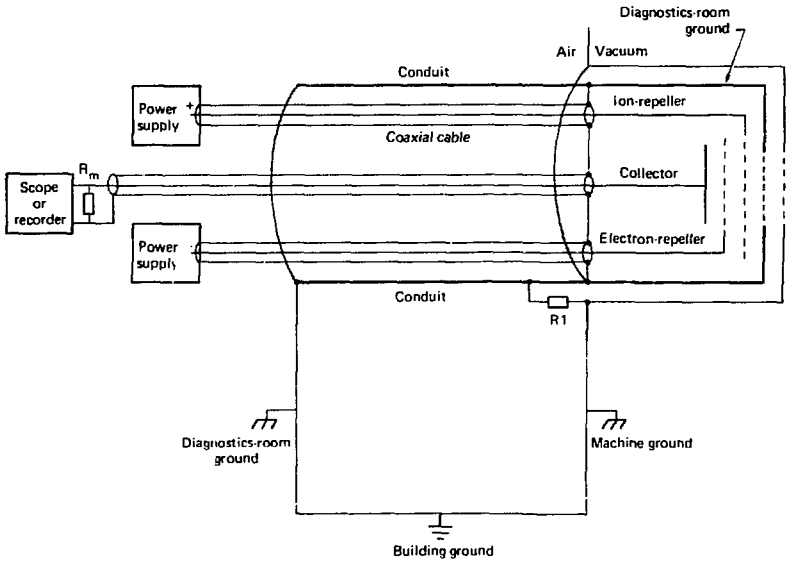

FIG. 5. The collector, grids, and coaxial cable connections to the scanning analyzer were electromagnetically shielded by being enclosed in a conduit that was a continuation of the analyzer case. (For simplicity, the electron suppressor grid and cable were omitted from this figure.) The entrance aperture opening in the case was closed by an entrance grid. An additional entrance grid and case at machine ground, that surrounded the analyzer, bypassed large plasma currents to ground and minimized perturbation of the plasma by the difference between ground potentials that could exist during injection by the streaming-plasma gun. Machine and diagnostics-room grounds were connected to the analyzer by R1 = 100 Ω, in addition to their independent and widely separated connections to building ground. This provided a low-impedance path for small signals, but limited ground-loop currents.

power supplies. The conduit was hard grounded only in the diagnostics room and was electrically isolated from the 2XIIB machine ground. To avoid drawing large currents from the streaming-plasma guns to the diagnostics-room ground, the case of the scanning analyzer was surrounded by another case and by an entrance grid, both of which were connected to machine ground (Figs. 2 and 5). The 5-cm analyzer and the multicollector design similarly used a machine-grounded grid and entrance tube to block most of the plasma current from flowing through the diagnostics-room ground. Rather than relying on the two widely separated inductive connections to building ground, diagnostics-room ground and machine ground were usually connected at the analyzer by a resistor (soft ground) of about 100 Ω that was small enough to provide a low-impedance current return for high-frequency plasma currents. On the other hand, the two grounds could differ by tens of volts for a few microseconds when the streaming-plasma guns were fired; then, 100 Ω was large enough to limit the ground-loop current to tolerable levels.

Oscilloscope traces from 2XIIB runs using the scanning analyzer (Fig. 6) show that the shielding reduced noise peaks to ±0.01 V from the much greater than 1-V ambient noise levels. Furthermore, the dynamic range between 100 μs when the signal comes out of saturation at a 1-V level, and 700 μs, when the signal approaches noise level of 0.01 V, was at least 100.

The four modes of grid biasing used on these analyzers are shown in Figs. 7(a) through 7(d). Figures 7(a) and 7(b) show typical grid biases for measurements of the ion current density at lower and higher space-charge limits, respectively. Figures 7(c) and 7(d) show typical grid biases for measuring electron current density at lower and higher space-charge limits, respectively.

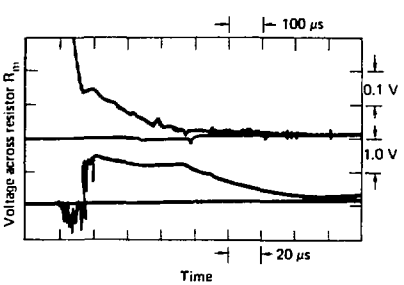

FIG. 6. The ion-collector current from the scanning analyzer is displayed vs time at two sweep speeds and vertical gains. Pulsed plasma guns were fired into the analyzer 20 μs after the oscilloscope was triggered. The current came smoothly out of saturation at 100 μs, then decayed to a level 100 times smaller at 700 μs before being lost in noise. The ion current density approaching the entrance grid was obtained from the traces by the conversion factor 4.0 A/(cm^2 • V).

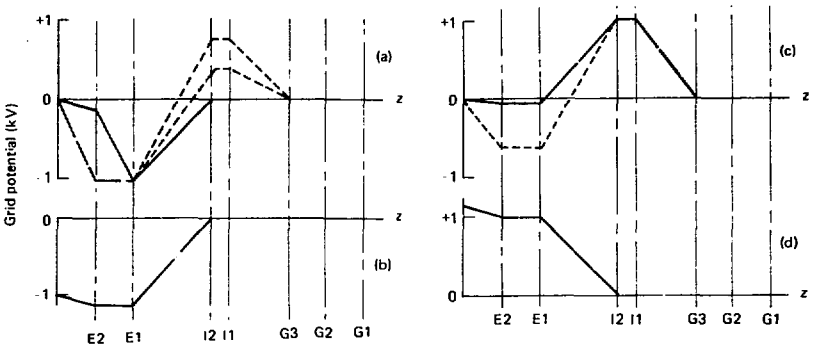

FIG. 7. Grid potential distributions for 2XIIB analyzers are shown. Grids G1 through G3 are grounded entrance grids: grid G1 is at 2XIIB machine ground; grids G2 and G3 are at diagnostics-room ground. (a) The double ion-repeller grids I1 and I2 are grounded (solid line) to measure the total current density of ions or biased (dotted line) to measure the current of ions above the bias energy. The electron repeller E1 is typically biased to -1 kV and the electron suppressor E2 (if separated from E1 as in the solid line for the scanning analyzer) is biased to -20 V to suppress secondary electrons from the collector C. The dashed line indicates the electron-suppressor/repeller bias for the 5-cm analyzer. No differences in performance were observed between the negative-grid biases shown by the dashed and solid lines. The collector is grounded through a meter resistor. (b) The collector is biased to -1 kV to maintain ions at high energy and hence to maintain a high space-charge-limited current density after the electrons have been electrostatically separated. The ions cannot now be energy analyzed without losing the higher current limit. (c) Electron energy distributions are measured by varying the electron repeller bias (dotted line) while the ion-repeller bias is maintained high to repel all but very energetic ions. Electron current measurements, without energy analysis, use an electron-repeller bias of 5 to 20 V (solid line), sufficiently negative to suppress secondary electrons from leaving the collector, but not negative enough to reflect the primary electrons. (d) The collector is biased positively to increase magnitude of the space-charge-limited current density.

Ion and electron energy distributions can be measured only at lower space-charge limits. The ion-collection modes are discussed in greater detail in Secs. II.C and II.D, and electron collection is discussed further in Sec. II.E.

Amplifier overload from plasma-gun injection was observed when the input voltage exceeded full scale on the oscilloscope by one to two orders of magnitude, but was well below the maximum allowed input voltage of the amplifiers. Most amplifiers recover from overload on a 1- to 10-ms time scale. Much quicker recovery is available with high gain differential or comparator amplifiers that carry a specification on overload recovery time of typically 1 to 10 μs.

II. ION-CURRENT MEASUREMENTS

Accurate ion-current measurements with gridded analyzers require care in several areas that are discussed in this section. These include grid transmission and collection of ions at all angles out to the maximum angle desired relative to the axis; design of the entrance grid to isolate the plasma from the analyzer potentials and attenuate the plasma flow; suppression of electrons originating from several sources; evaluation of the space-charge limits on the current and discussion of techniques for increasing the limits; effect on design criteria necessitated by the collection of electrons rather than ions; and the mapping of the measured ion current density to any point along the magnetic flux tube.

A. GRID TRANSMISSION AT LARGE ACCEPTANCE ANGLES

A large acceptance angle was required for 2XIIB analyzers in order to measure all ions that were not confined by the magnetic mirrors. We calculated the acceptance angle as follows:

Scattered ions are lost primarily because of small-angle collisions that have left them near the periphery of the loss cone; however, the streaming plasma is expected to fill the loss cone.[2] The loss-cone angle is calculated from conservation of energy

$$E_{\perp} + E_{\parallel} + q\phi = E \qquad (1)$$

and the adiabatic invariant μ,

$$\mu \equiv E_\perp / B \quad , \tag{2}$$

where $E_\perp$ and $E_\parallel$ are the ion energies, transverse and parallel to the axial magnetic field, respectively, ϕ is the plasma potential (expected to be a few hundred volts), q is the ion charge, and B is the magnetic field strength. The adiabatic invariant μ is constant as long as the magnetic field is nearly uniform over an ion orbit.[7] The ion with the largest angle will be one that has almost all transverse energy at the magnetic mirror ($E \approx E_\perp = B_m$), and hence is barely transmitted. Then, the angle θ between the ion trajectory and the magnetic field at the analyzer (B_a) is given by

$$\theta = \arctan\,(E_\perp / E_\parallel)^{1/2} = \arctan\left\{B_a/[B_m - B_a - (q\phi/\mu)]\right\}^{1/2} \quad , \tag{3}$$

where B_m is the magnetic field at the mirror. For typical 2XIIB parameters where B_m = 13 kG and $B_a \leq$ 2 kG, we obtain $\theta \leq 23^\circ$. If we assume that unconfined ions at the hot plasma are isotropic, then in 2XIIB the average ion angle at the analyzer was 16° from axial.

The angular acceptance requirement affects two aspects of analyzer design. One aspect, the transmission of grids at large angles, is necessary for both current and energy measurements; the other, the confinement of ions with large perpendicular energy, is necessary only for energy measurements, and is discussed in Sec. III.A. To maximize the angular acceptance for 2XIIB, we proceeded as follows:

We chose flat, electroplated mesh grids rather than woven or knit grids. In addition to having all the wires in one plane, electroplated grids have slightly conical holes that provide a greater acceptance angle than would cylindrical holes.

The net transmission of multiple grids is determined from the individual grid transmissions. A broad angular distribution of ions transmitted through a set of apertures separated transversely by much less than an ion gyroradius will have lost all memory of the pattern of one grid before reaching the next grid located axially many grid-aperture separations distant. Then the total grid transmission is the product of the individual grid transmissions:

$$T_T = T_1 \cdot T_2 \cdot \cdot \cdot T_n \quad . \tag{4}$$

To maintain the validity of Eq. (4) and to avoid preferentially transmitting only part of the angular distribution due to the relative alignment of grid holes, subsequent grids have closer hole spacing than does the first entrance grid, and are separated from adjacent grids by much more than the hole separation times the cotangent of the ion trajectory angle. (This condition was met on 2XIIB, but is difficult to achieve with the highly collimated ions from TMX.) The absence of Moiré fringes is a convenient criterion for selecting pairs of grids to be used with a close spacing. The presence of fringes indicates that the grid transmission will vary with the angle of incidence and with grid alignment. The variation becomes greater as the size and contrast of the fringes increase.

A figure of merit α for the angular transmission, with an average angle of 16°, is given by

$$\alpha(16^{\circ}) \approx \left[T_T(16^{\circ})/T_T(0^{\circ})\right] \quad . \tag{5}$$

Obviously, our goal is to maximize α to as near unity as possible. We achieve $\alpha = 0.67$ with the scanning analyzer [as can be calculated from data in Table 1 by means of Eqs. (4) and (5)] and $\alpha = 0.82$ with the 5-cm analyzer by choosing grids that are thin compared to the aperture diameters. This requirement must be balanced against other conflicting requirements to be discussed in Sec. II.B. The transmission of individual grids was determined by measuring the transmitted light to a photomultiplier tube. These measurements were made at 0° and 16° from normal to the grid. Table 1 shows results for the scanning analyzer.

Ensuring that all ion trajectories end at the collector is trivial if only the total ion current is to be measured. Then, it is only necessary that the collector, grids, and entrance tube (if any) subtend larger solid angles from the entrance aperture than do the ion trajectories. However, further considerations are necessary if the ion energy distribution is to be measured, as is discussed in Secs. III.A and III.B.

B. ENTRANCE-GRID DESIGN

The multiple, grounded entrance grids accomplish several functions that are essential to the correct performance of these gridded analyzers.

- They establish a ground potential that isolates the plasma outside the analyzer from perturbation by biased repeller grids.[6] This requires

tenuating the plasma density so that the Debye length exceeds the mesh size of the grid.

- They reduce the ion current density below the space-charge limit, (as discussed in Sec. II.D).

- They attenuate the power density below the value at which the interior grids would overheat and warp. However, the thick entrance grids that absorb this power without warping or melting must maintain wide angle transmission.

- Finally, they withstand metal deposition from titanium gettering without significantly altering their transmission.

In some cases, less than optimum performance must be accepted in one function in order to achieve adequate performance in another.

The entrance grids at diagnostics-room ground, as well as the repeller grids of the analyzers, must have hole radii that satisfy the criterion $r_0 < \lambda_D$. The Debye length λ_D is determined by the plasma density n_e and the electron temperature T_e to be[7]

$$\lambda_D \text{ (cm)} = 700 \left[T_e \text{ (eV)}/n_e \text{ (cm}^{-3})\right]^{1/2} . \quad (6)$$

In Table 1, we list the density allowable at any grid of the scanning analyzer. To ensure that we do not exceed the density rating of any grid, we use the following procedure. We begin by calculating the maximum density ($n_e = 2.1 \times 10^{10}$ cm^{-3}) allowed by Eq. (6) for $T_e \geq 20$ eV at the last grid E2 before the collector. The allowed density at the preceding grid E1 is the lesser of $n_e(E1) = n_e(E2)/T(E1) = 2.8 \times 10^{10}$ cm^{-3} and n_e as calculated from Eq. (6) for $r_0 = \lambda_D$ ($n_e = 2.1 \times 10^{10}$cm^{3}). In this manner, always taking the lesser of the calculated densities, we calculate that a density of $n_e = 1.2 \times 10^{13}$ cm^{-3} at the first entrance grid G1 is the maximum that does not result in exceeding the maximum density rating of any grid in the scanning analyzer. This ensures that the plasma does not shield grid potentials from the ions, thereby allowing transmission of ions with axial energy below the potential of the ion-repeller grid.

We can ensure that repeller grid potentials do not perturb the plasma outside the analyzer by requiring that two grounded entrance grids have mesh openings of less than one Debye length.[6] This is accomplished as discussed above for $n_e < 1.2 \times 10^{13}$ cm^{-3}. But we do not need to place this requirement on the first entrance grid, because that grid serves primarily to reduce the incident power and current density.

Selecting an entrance grid requires compromises between two further requirements: the grid must be thin relative to the hole size to allow for wide angular transmission, but it must also be thick in order to absorb thermal energy. The first two entrance grids in the scanning analyzer were thick enough, 180 μm and 100 μm, respectively, to absorb 10 J/cm^2 during a 10-ms-duration plasma shot on 2XIIB without melting or warping. Together, they attenuated the plasma by a factor of 320, to limit the temperature rise of the 5-μm-thick repeller grids to less than 15°C.

A possible pitfall in such large attenuations is that rather than a uniform decrease in ion density, one obtains isolated high-density beamlets that locally violate the Debye length and space-charge limits (Sec. II.D) on density and current density, respectively. The attenuation by subsequent grids could then be a function of the alignment of grids relative to one another. We can avoid these problems by choosing a first grid with holes separated by no more than two electron gyroradii ($\rho_e = m_e v_\epsilon / qB_a = 80$ μm for 20-eV electrons and $B_a = 2$ kG) so that electron as well as ion beamlets merge between grids. This condition is easily met on TMX, but could not quite be achieved on 2XIIB. Small grid holes separated by large distances also eliminate electrostatic lens effects that can change the angular distribution, distorting the relationship between axial and transverse energy[4] (Sec. III.D).

Electroplated grids such as those for the scanning analyzer described in Table 1 come closest to satisfying these contradictory requirements for high attenuation and high power absorption, yet wide angular transmission. The transmission of electroplated grids can be reduced and the strength increased by purchasing grids plated up to greater thicknesses on one side only. The metal tends to close up the holes as it plates; the conical holes thus produced reduce the angular transmission to a lesser degree than would cylindrical holes.

The holes in the first entrance grid are large, 180 μm in diameter, so that the deposition of up to 10 μm of titanium gettering will not change the transmission by more than 10%.

C. ELECTRON SUPPRESSION

Depending on where they originate, collected electrons can produce errors in ion current measurements and distort ion energy distributions. These

electrons include the primary electrons and also secondary electrons resulting from electron, ion, or photon bombardment of grid supports, the collector side of grids, or the collector itself. Note that with ion energies exceeding 100 eV, secondary electrons from ions must be considered as carefully as those resulting from the impact of electrons on surfaces.[8]

Primary electrons must be prevented from reaching the collector. Primary electrons can reach the collector if the electron-repeller grid is not biased sufficiently negatively (Fig. 8), if the grid apertures are much larger than a Debye length, or if the current density exceeds the Child-Langmuir space-charge-limited current (Sec. III.D). Checking that primary electrons are repelled is necessary as experimental conditions change.

Either a double electron-repeller grid (in the 5-cm analyzer, Fig. 3) or a secondary electron suppressor plus a repeller grid (in the scanning analyzer, Fig. 2) has been used to provide a better shield between the collector and a swept-ion repeller grid. No difference has been observed in the performance of these two designs. However, capacitive coupling was observed in the scanning analyzer between a swept-ion repeller and the collector when they were separated by a single grid. Using two electron-repeller (suppressor) grids reduced the coupling to an imperceptible level.

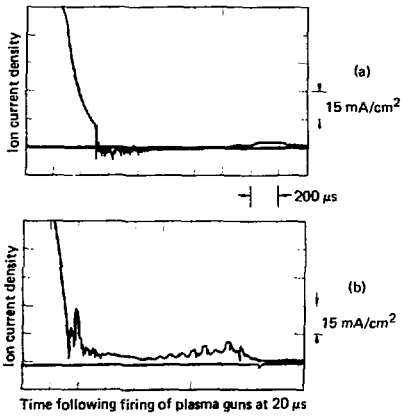

FIG. 8. In these results from a 2XIIB run using the scanning analyzer, electron-repeller grid biases of -500 V and -600 V were inadequate to stop primary electrons in (a) when a streaming-plasma gun fired at 500 μs. Increasing the biases to -600 and -700 V in (b) stopped electrons, eliminating the anomalously low or negative ion-currents. Further increasing the electron repeller bias had no additional effect.

The most important technique for minimizing the collection of secondary electrons is to make the diameter of the collector less than the open diameters of the electron-repeller and secondary-suppressor grids (Figs. 2 through 4). This prevents secondary electrons from flowing from the negative grid supports along the axial magnetic field to the collector. Secondary electrons from other grounded or positive grids and supports are stopped by electron-repeller suppressor grids immediately before the collector. An earlier analyzer with a collector diameter greater than the grid diameters produced measurements similar to those of Fig. 8(a) because secondary electron currents from grid supports exceeded the ion current to the collector.

In this technique, referred to as magnetic insulation,[9] a magnetic field is strong enough, for a given transverse electric field, to bend electrons back to the emitting surface without their reaching the collector. The minimum distance $d = r_e - r_c$ required between the radii of the suppressor grid and the collector, respectively, is given by[9]

$$d = \left[2m_e V_e/(q\,B^2)\right]^{1/2} \qquad (7)$$

where V_e is difference between the bias voltages of the electron repeller and the collector, and m_e is the electron mass. This criterion is easily satisfied on 2XIIB, but not on TMX; it is conservative in that its derivation assumes that the total electric field E, rather than only one component, is perpendicular to B.

We chose to locate the negative electron-repeller grids after the ion-repeller grids (Figs. 2 through 4, 7) so that they would repel the secondary electrons from other grids. Ions reflected by the ion-repeller potential create secondary electrons off the downstream sides of preceding grids. These secondary electrons reach the collector if they originate on the negative electron-repeller grids, but are stopped by subsequent negative grids if they originate on grounded or positively biased grids. Such secondaries reaching the collector not only produce errors in the value for the total collected ion current but also distort the ion energy distribution because the secondary electron current is proportional to the ion current reflected by the repeller grid. When mounted next to the collector, the electron-repeller grids also suppress secondary electrons off the collector.

Only secondary electrons created on or after the most negatively biased grids, the electron-repeller/suppressor grids, can reach the collector. Secondaries originating on the upstream side of the negative grids will be repelled away from the collector, and ions or electrons cannot strike the downstream side of these grids; however, secondaries created on the edges of grid holes can be collected. We minimize these by choosing the electron-repeller/suppressor grids to be as thin and transparent as possible. Biasing the second electron-repeller grid so that it is more negative than the first can reduce the number of secondaries from the first electron-repeller grid that reach the collector. We tried this grid bias arrangement with the scanning analyzer, but could detect no difference from operation with the bias arrangement shown in Fig. 7(a).

Photoelectrons reaching the collector from the grids remain a possible source of error in ion current and energy measurements. Reflection of ultraviolet light by the collector to the downstream side of the negative grids produces secondary electrons that are collected. The reflection can be reduced by coating the collector with a low-reflectivity, low-Z material such as carbon. If necessary, the reflectivity of the collector could be further reduced by giving the collector a multiple deep "V" surface that would subject the light to multiple reflections before it escaped. On 2XIIB analyzers, we used both carbon-coated and matte-finish stainless-steel collectors. We observed no differences attributable to photoelectrons.

In magnetic field-free analyzers, secondary emission from the collector can be minimized by using a deep Faraday cup in which the entrance subtends a small solid angle from the collection surface and emitting surfaces are shielded from electric fields. This reduces the loss of secondary electrons. However, because in the analyzers discussed here the axial magnetic field confines the secondary electrons to the emission area, a deep collector cup provides little advantage over a flat collector plate. Therefore, a flat collector preceded by (Fig. 3) or surrounded by (Fig. 2) a suppressor grid is used in these analyzers.

D. SPACE-CHARGE LIMITS

Despite the large plasma attenuation by the entrance grids, the space-charge-current limit of the 2XIIB analyzers was exceeded when streaming plasma

was injected as gas at the nearest magnetic mirror rather than from a gun at the opposite end of 2XIIB.[10] Currents beyond the limit of the analyzer produced negative current spikes similar to those in Fig. 8(a). One solution was to decrease the current density in the analyzer by introducing an additional 0.023 transmission entrance grid.

A second solution is to increase the limit of the current by space charge that rises near the collector [curve (a) in Fig. 9]. Here, the positive space charge of the ions, after the electrons neutralizing the space charge have been reflected, becomes large enough to reflect ions of energy $E_{\parallel} < qV_m$. This limit can be increased by biasing the collector negatively [curve (b) in Fig. 9]. The latter helps in two ways: the minimum kinetic energy of ions is increased to the initial energy $E_{\parallel}$ plus the magnitude of the bias potential qV rather than decreasing to or below $E_{\parallel}$; and the space charge of the ions is lower by $(qV + E_{\parallel})^{1/2}$ because of the higher ion velocity at a fixed ion current. These two effects give the $V^{3/2}$ dependence of the Child-Langmuir space-charge-limited current[11] for deuterium ions.

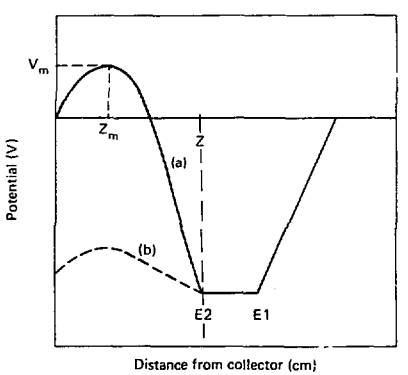

FIG. 9. The ion current becomes space-charge limited if the ion space-charge potential V_m exceeds the axial ion energy $E_{\parallel}$ [curve (a)]. The ion current limit is increased by biasing the collector negatively to collect ions at higher energy than $E_{\parallel}$ and to reduce V_m below any $E_{\parallel}$ of interest [curve (b)].

This problem is equivalent to that analyzed by Langmuir, except that we consider ions decelerating rather than accelerating towards the collector. In either case, the critical current occurs when the ion velocity approaches zero at V_m; hence, the ions are barely transmitted. Langmuir[11] derives the critical current, which for deuterium ions is

$$j \approx 3.85 \times 10^{-8} \frac{(qV + E_{\parallel})^{3/2}}{(z - z_m)^2} \left[1 + 0.0247\, T^{1/2}(V + E_{\parallel})^{-1/2}\right] , \qquad (8)$$

where j is in A/cm^2, qV is in eV, z is the grid separation in cm, $(z - z_m)$ is the distance between the minimum and maximum potential in cm, and T is the ion temperature in eV. The initial average ion energy $E_{\parallel}$ is in the range 100 to 400 eV. Increasing the collector bias V from 0 to 1000 V [curve (b) of Fig. 9] increases the space-charge limit of the scanning or the 5-cm analyzers by a factor of 6 to 36, or by more if the change in $(z - z_m)$ is included.

The circuit used for biasing the collector is shown in Fig. 10. Most of the circuit design is necessitated by the lethal 50 J stored in C2. Passive protection is provided by a bleed resistor R2. Active protection is provided by the vacuum relay crowbar that discharges the capacitor through a wire-wound resistor R3. To prevent a blown meter resistor from opening the capacitor discharge path, the meter resistor R_m was placed at high voltage, then capacitively coupled to either an oscilloscope or a digital recorder. The coupling capacitors C1 were chosen large enough to drive a 1-MΩ load with a minimal voltage drop to the end of the pulse, and were chosen to have low inductance for good frequency response.

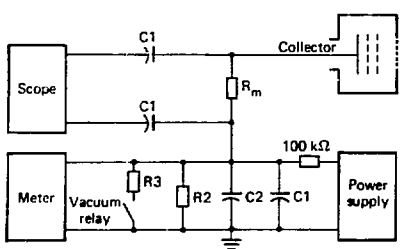

FIG. 10. The collector bias circuit is used to increase the space-charge-limited current. Component values used were R_m = 10 Ω; C1 = 1-μFd (low inductance), C2 = 100-μFd (electrolytic), and R2 and R3 are safety discharge resistors (R3 = 10 kΩ, 10 W, and R2 = 1 MΩ, 1 W).

The space-charge-limited ion current at the ion-repeller grid is slightly larger than at the collector because electrons are still present to neutralize space charge. The increased space-charge limit on the ion current is given by the ratio of the ion density n_i to the net charge density $(n_i - n_e)$:

$$j'/j = n_i/(n_i - n_e) \quad . \tag{9}$$

We evaluate Eq. (9) for an ion-repeller grid bias equal to a typical plasma potential of 200 V. The average end-loss ion energy of 400 eV is the sum of the plasma potential plus the axial temperature $T_{\parallel}$, 200 eV. The incident electron flux satisfies $j_e = j_i$ (for a nonemitting end wall) and $n_e = n_i$. Then, for $n_i = j/qv_{\parallel}$ and $1/2\ mv_{\parallel}^2 = T_{\parallel}$,

$$j'/j = \left[1 - \left(\frac{T_{\parallel}}{\phi_p}\frac{m_e}{m_i}\right)^{1/2}\right]^{-1} \approx 1.02 \quad . \tag{10}$$

A change of three orders of magnitude in any one of the assumptions would be necessary to double the space-charge limit. This effect is small because, although ions and electrons enter the analyzer with equal space charge and current, the ions are retarded and the electrons accelerated by the ion-repeller grid. Therefore, the relative electron space charge near the ion-repeller grid is small. From this result, we conclude that ion or electron energy distributions cannot be accurately measured at the high current densities possible with the bias arrangements of Figs. 7(b) and 7(d).

E. ELECTRON-CURRENT MEASUREMENTS

Electron currents are measured with analyzers biased as in Figs. 7(c) and 7(d). The positive bias is high enough to repel most ions. Secondary electrons from the collector are suppressed by the slightly negative, adjacent suppressor grid. The electron energy is measured by varying the bias on the electron-repeller grid, as indicated by the dotted lines in Fig. 7(c). This arrangement of biases also reduces the instrumental error ensuing from the collection of secondary electrons off grids because only electrons from the electron-repeller grids can reach the collector. The alternate bias arrangement, Fig. 7(d), increases the space-charge limit of the electron current, but the analyzer then can neither analyze electron energy nor suppress secondary electron current emitted from every grid.

F. CURRENT MEASUREMENTS MAPPED TO PLASMA

The current density j_p at the plasma is calculated from that at the analyzer entrance grid j_a, assuming that the current density mapping follows that of the magnetic field,

$$j_p = j_a \, B_p/B_a \quad , \tag{11}$$

where B_p is the magnetic field at the plasma, and $B_p \approx 0.5 \, B_m$ in 2XIIB and TMX. If the plasma pressure is comparable to the magnetic field pressure (high beta), then appropriate reductions must be made in B_p.

The current density at the entrance grid is determined from the collector current I_c through a meter resistor, the grid transmissions T_T (16^o) for the average ion at 16^o from normal in 2XIIB or $T_T(0^o)$ in TMX [see Eqs. (4) and (5) and Table 1], and the entrance aperture area A_a:

$$j_a \ (A/cm^2) = \left[I_c(A) / \ A_a(cm^2) \ T_T(16^o) \right] \quad . \tag{12}$$

The total grid transmission is measured optically as discussed in Sec. II.A.

End-loss current profiles in 2XIIB were measured by moving the entrance aperture of the scanning analyzer between shots. In Fig. 11, the current is mapped along magnetic field lines to the center of the plasma, where it is compared with the radial density profile of the hot plasma.[12] The unconfined plasma profile is seen to be similar to but slightly wider than the hot-plasma profile.

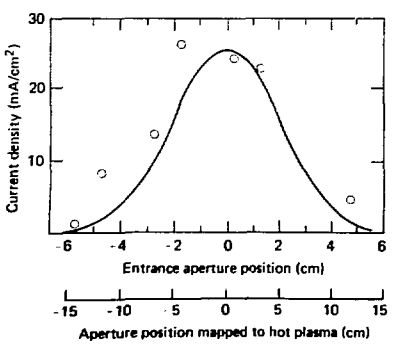

FIG. 11. The end-loss current profile in 2XIIB, shown by data points, was measured across the minor diameter of the plasma by moving the entrance aperture between shots. The abscissa includes the actual aperture location at z = -330 cm and the aperture position mapped along magnetic field lines to the center of the hot plasma at z = 0. For comparison, the solid line shows the best-fit Gaussian curve to the measured density profile of the hot plasma.

III. ION ENERGY DISTRIBUTIONS

We have already discussed several causes of errors in measurements of the ion energy distribution. These include the angular transmission of the grids, secondary electrons from ions reflected by the ion-repeller grid, and space-charge effects. Other causes of errors in measurements or their interpretation that will be discussed here include: ion trajectories that miss the collector, the angular transmission of the ion-repeller grid, the fact that these analyzers measure axial energy rather than axial momentum,[4] the relationship between axial and total energy, the alignment of grids normal to the magnetic field, lens effects, the influence of double versus single grids,[6] and ion-repeller sweep rates.

Backscattering of ions by the collector also reduces the collector current and distorts the measured ion energy distribution because increasing the bias of the ion-repeller grid returns backscattered ions to the collector. But, since backscattered ions have lost energy, they are reflected back to the collector by ion-repeller biases too low to stop the primary ions, thereby distorting the measured ion energy distribution. However, measurements presented in Sec. III.E show that this is not a major influence.

A. LARGE-ANGLE ION TRAJECTORIES

As ions are retarded in order to determine their energy distribution, they escape radially because the axial ion velocity approaches zero while the transverse velocity remains constant. Ion trajectories making large angles to the axis must be confined by the axial magnetic field in order to be analyzed. We confine them by requiring that the radii of the collector r_c, the electron repeller, and the ion-repeller grids all be larger than the radius r_a of the entrance aperture by one gyrodiameter ($2\rho_i$) of a maximum energy ion:

$$r_c = r_a + 2\rho_i \quad . \tag{13}$$

This requirement for measuring ion energy distributions is more stringent than that for measuring only the current (Sec. II.A). The radii of the electron- and ion-repeller grids are larger than that of the collector (Sec. II.C). The

adiabatic ion having the largest possible orbit will be one that escapes over the magnetic mirror with nearly zero axial energy; i.e., $E \approx E_\perp = \mu B_m$. We obtain the ion gyroradius at the analyzer:

$$\rho_i = \frac{m_i v_\perp}{qB} = \frac{1}{q}\left(\frac{2m_i E}{B_m B_a}\right)^{1/2} . \qquad (14)$$

Ions of energy up to E will be confined by the magnetic field at the analyzer B_a to a radius of no more than r_c. By conservation of energy [Eq. (1)], the ion-retarding grid can then analyze the ion energy parallel to the magnetic field independently of the perpendicular energy. This will be discussed further in Sec. III.D.

Grid diameters in the scanning analyzer (Fig. 2) and the multiple-collector analyzer (Fig. 4) are increased by the requirement that Eq. (13) hold for the corners of the entrance aperture in its extreme positions.

The energy resolution $\Delta E_\parallel$ can also be limited by the angular acceptance of the ion-retarding grid. An infinitesimally thin grid transmits ions up to 90° from normal. As the grid thickness increases, the grid transmission goes to zero at smaller angles, and ions require higher axial energy to be transmitted. This puts an upper limit on the allowable grid thickness δ compared with the hole radius r_0: $\delta = 2r_0 (\Delta E_\parallel / E_\perp)^{1/2}$. This criterion was easily met for a resolution $\Delta E_\parallel / E_\perp = 10^{-2}$ in 2XIIB and is even less of a problem for TMX, where the transverse energy of the ions is much less than the axial energy. This angular acceptance requirement for the ion-repeller grid is much more stringent than that for the entrance grid (Sec. II.B), but it is more easily met because the ion-repeller grid is not required to attenuate the plasma and absorb energy; hence, it can be a thin, high-transmission grid.

It is ironic that the axial magnetic field not only solves but also creates the problem of a wide angular distribution of ions, for without a magnetic field, ion trajectories from a distant source are well collimated if both the analyzer aperture and the source subtend small solid angles relative to each other. This collimation is required by and available to magnetic-field-free analyzers.[4] However, with an axial magnetic field extending from the source to the analyzer, the angle between an ion trajectory and the axis can be as large as 90° if the ratio of the magnetic field strength at the analyzer to that at the plasma is unity, or can approach 0° if the field ratio approaches zero [Eq. (3)]. With a magnetic field ratio of order 10^{-1}

or greater, it is necessary to capitalize on the magnetic field in order to confine the orbits of uncollimated ions within the analyzer.

The axial magnetic field is essential to obtaining the wide angular acceptance of these gridded analyzers; however, lowering the magnetic field at the analyzer reduces this need and provides several other advantages:

- Insofar as ions and electrons follow magnetic field lines, the conservation of magnetic flux then spreads the plasma over a larger area.
- The current density j_a at the analyzer is then reduced from that at the plasma j_p [Eq. (11)].
- The ion density and power density are similarly reduced, allowing coarser grids to be used.
- The angular spread of the ions is also reduced [Eq. (3)], allowing thicker grids to be used.
- The spacing of grid holes can be increased without exceeding two electron-gyroradii (Sec. II.B).

However, lowering the magnetic field at the analyzer provides two disadvantages: in order to contain ion orbits, either the radius of the analyzer must scale as $r \propto B_a^{-0.5}$ [Eq. (13)] or adequate ion energy resolution must be ensured by collimating ion trajectories; and the diameter of the suppressor grid must be sufficiently larger than the collector diameter to prevent the collection of secondary electrons from the grid supports across the magnetic field [Eq. (7)]. As we will discuss in the next section, ion trajectories are well collimated on TMX,[3] where these advantages allow simpler analyzers to function.

B. COLLIMATED ION TRAJECTORIES

Adequate energy resolution can be attained with smaller-diameter analyzers than those required by Eqs. (13) and (14) if the ions are collimated to have trajectories nearly parallel to the magnetic field. Collimation is either achieved by means of apertures or, as in the case of the TMX, by reducing the magnetic field from 20 kG at the mirror to 70 G at the analyzer. This reduces the angle that adiabatic ions make with the axial magnetic field in TMX to a maximum of 3.4° [Eq. (3)]; 2XIIB ions made a 23° angle.

The design of simple retarding analyzers to measure the energy distribution of collimated ions is discussed in the literature[4] for magnetic-field-free

analyzers. Since any substantial relaxation of the Eq. (13) criterion results in ion orbits larger than the analyzer, we assume zero magnetic field to provide straight ion trajectories in the following analysis.

The energy resolution of magnetic-field-free analyzers is limited because some ion trajectories miss the collector. The electric field from the ion-repeller grid is parallel to the magnetic field; hence, it retards the axial velocity of the ions but the transverse velocity $v_\perp$ remains constant. We define the critical time of flight t_c from the entrance aperture to the collector of radii r_a and r_c, respectively, for which the collector barely intercepts the ion:

$$t_c = (r_c - r_a)/v_\perp \quad . \tag{15}$$

We define the axial energy uncertainty $\Delta E_\parallel$ to be

$$\Delta E_\parallel = E_\parallel - qV \quad , \tag{16}$$

where $E_\parallel$ is the axial energy of an ion that barely misses the collector, and V is the voltage of the ion-repeller grid. We calculate the energy uncertainty by computing the axial time of flight from the entrance aperture to the collector and equating that time to t_c. As shown by the dotted lines of Fig. 7(a), an ion enters from the right, maintaining uniform axial velocity through the last entrance grid G3. It then decelerates to the first ion-repeller grid I1, and travels at a uniform velocity $v_a = (2\Delta E_\parallel/m_i)^{1/2}$ the distance Δz to ion-repeller grid I2. From I2, it accelerates to the electron-repeller grid E1, coasts or decelerates to E2, then finally decelerates to the collector. For $\Delta E \ll E_\parallel$, the time of flight depends on ΔE only between the double ion-repeller grids. We write the axial time of flight t_A as the sum of the time of flight through the ion-repeller grid, $\Delta t_i = \Delta Z\ (m_i/2\ E_\parallel)^{1/2}$, plus the time of flight through all the other regions t_c'; i.e., $t_A = \Delta t_I + t_c'$. Equating t_A to t_c from Eq. (14) and solving for ΔE, we obtain

$$\Delta E = E_\perp \left(\frac{\Delta z}{r_c - r_a - v_\perp t_c'} \right)^2 \quad , \tag{17}$$

where $E_\perp = 1/2\ m_i v^2$. The energy uncertainty is minimized either by maximizing r_c or by minimizing the transverse ion energy, the separation beween the double ion-repeller grids, the diameter of the entrance aperture, or the total

distance from the entrance to the collector to minimize t'. For an ion energy of 400 eV in TMX, we obtain $\Delta E_{\parallel} \ll 1$ eV, which is more than adequate accuracy.

Analyzers with high axial energy resolution can be designed from Eqs. (13) or (17). Equation (13) is generally valid and must be used to obtain high-energy resolution with uncollimated ions (as in 2XIIB) where Eq. (17) would be invalid. With collimated ions (as in TMX), either equation is valid, but Eq. (17) usually permits a smaller-diameter analyzer.

C. VOLTAGE SWEEP-RATE LIMITS

In addition to allowing the ion to miss the collector because of the finite transverse velocity of the ions, the axial time of flight can also reduce the energy resolution in a second way. If the ion-repeller grid bias is swept, the bias will have changed during the ion time of flight t_{Ic} from the ion-repeller grid to the collector. The energy resolution $\Delta E_{\parallel}$ of an analyzer repeller grid swept at a rate dV/dt is then given by

$$\Delta E_{\parallel} = q t_{Ic} \frac{dV}{dt} \quad . \tag{18}$$

We compute the time of flight through double repeller grids separated by 0.3 cm to be 10^{-7} s for a resolution $\Delta E_{\parallel} = 10$ eV. The total time of flight of a deuterium ion from the first ion-repeller grid to the collector is 1.7×10^{-7} s in the scanning analyzer and 1.4×10^{-7} s in the 5-cm analyzer. This allows ion-repeller sweep rates of $dV/dt \leq 6 \times 10^{7}$ V/s and $dV/dt \leq 7 \times 10^{7}$ V/s, respectively, with 10-eV resolution at 400-eV axial ion energy. Further increases in sweep speed or resolution are limited primarily by the time of flight through the double grids because these grids must be separated by several mesh diameters to minimize lens effects[6] and to ensure that no electric fields penetrate the grid. Single grids that allow potentials to penetrate do not produce the sharp energy cutoff of double grids,[6] but if a very fast sweep is required, the net ion energy resolution could be higher with a single grid because of the shorter time of flight. Small reductions in time of flight are possible if we reduce the gaps between grids other than the double ion-repeller grid.

D. AXIAL VERSUS TOTAL ENERGY

The relationship between axial and total energy at the loss-cone angle is given by Eqs. (1) through (3). In a uniform axial magnetic field normal to the grids and parallel to the retarding electric fields, the transverse energy is constant. Then, from conservation of energy [Eq. (1)], we measure the axial energy with these retarding potential analyzers. Other analyzers measure axial momentum: Simpson[4] considers an analyzer with two limiting apertures, both smaller than an ion or electron orbit. In that analyzer, only particles making small angles to the axis plus those in certain angular bands are transmitted. Simpson[4] also points out that, with a uniform magnetic field from the source of ions to the analyzer, an axial energy measurement may tell nothing about the total energy unless the angular distribution is also known. Again, our case is different because the magnetic field at the analyzer is reduced from that at the hot plasma, the result being conversion of most of the transverse energy into axial energy [Eqs. (1) through (3)]. For example, in 2XIIB we obtain $E_\perp/E_\parallel \leq 0.18$; and in TMX, $E_\perp/E_\parallel \leq 3.5 \times 10^{-3}$. Hence, although only the axial energy is measured, the total energy can be inferred with reasonable accuracy.

Lens effects can deflect ions from their trajectories, thereby mixing axial and transverse energy as ions pass the grid wires. These effects have been analyzed by Simpson[4] and by Stephanakis and Bennett.[6] Simpson derives the relative error in measuring total energy as

$$\Delta E_\parallel/E_\parallel = r_0^2/(16z^2) \quad , \tag{19}$$

where r_0 is the mesh opening and z is the distance between grids. For the grid parameters listed in Table 1, where grids at different potentials have a minimum gap of 1.0 cm, the maximum error is $\Delta E_\parallel/E_\parallel \approx 2 \times 10^{-5}$, which can be neglected.

Axial and transverse energy will also be mixed if the ion-repeller grids and adjacent grids are not everywhere normal to the magnetic field. Then, because the electric field has a component transverse to the magnetic field, the ion-repeller grids reduce the transverse as well as the axial energy. For grids at an angle γ from normal to the magnetic field and ion trajectories at an angle θ to the magnetic field, we obtain at the ion trajectory extrema

$$\Delta E_{\parallel}/E_{\parallel} = [1 - \cos^2 (\gamma \pm \theta)]/\cos^2 \theta \quad . \tag{20}$$

For the analyzers described here, this error is also small. These analyzers were built with grids parallel to within 1°. Furthermore, the scanning analyzer was installed in the center of solenoidal coils, at an axial position where the direction of the magnetic field lines varied by $\gamma < 0.5^{\circ}$ from normal over the 25-cm diameter of the grid. When mounted in a port normal to the field line, the 5-cm analyzer is also small enough to satisfy $\gamma < 0.5^{\circ}$. The maximum deviation of magnetic field lines from normal to grids is therefore comparable to or less than 1.5° in both analyzers. Thus, for $\theta = 23^{\circ}$ in 2XIIB, the error is less than 2.2%; for $\theta = 3.4^{\circ}$ in TMX, the error is less than 0.7%.

E. EXAMPLES OF ANALYZER MEASUREMENTS

Some capabilities of the analyzers are demonstrated in the figures accompanying this report: ion energy measurements are shown in Figs. 12 through 14, current measurements were shown on Figs. 6, 8, and 11.

The energy resolution of the scanning analyzer (Fig. 12) was measured with radio-frequency (rf) ion source installed at the position of the streaming-plasma gun (see Fig. 1). Two conclusions were drawn from these data. First, the analyzer resolution was $\Delta E_{\parallel}/E_{\parallel} \leq 0.022$ at 1580 eV. Because this resolution was adequate, we made no attempt to separate the instrumental resolution from the width of the distribution produced by the rf ion source. Second, no variation in collector current was observed from 0 to 1500 eV, indicating that ion backscattering from the collector was not significant. If ions were reflected, we would expect them to emerge from the collector at less than 1580 eV. Those that did not intercept the electron suppressor grids would be reflected back to the collector by the ion repeller--until the bias of the ion repeller was reduced below the energy of the reflected ions, at which time the collector current would begin to decrease. Since no such decrease was seen, we conclude that reflection of 1580-eV ions is less than the $\pm 5\%$ variation in the output of the rf ion source.

Energy distributions $f(E_{\parallel})$ of end-loss ions have been measured both by changing the bias of the ion repeller from shot to shot (Fig. 13) and by

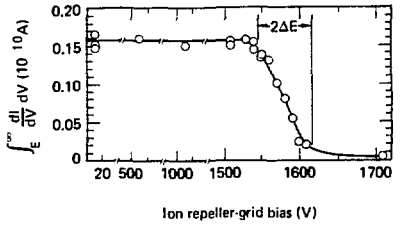

FIG. 12. The energy resolution of the scanning analyzer was measured with an rf ion source to be $\Delta E/E \leq 0.022$. Backscattering of 1580-eV ions from the collector would produce a smaller current at 0 V than at other bias voltages below 1530 eV. Backscatter was less than the ±5% drift of the ion source.

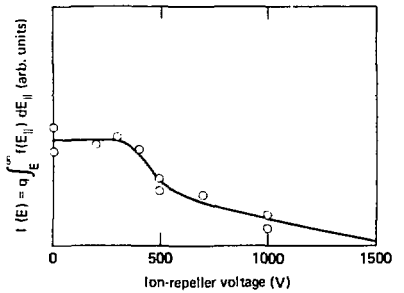

FIG. 13. The ion energy distribution $f(E_{\parallel})$ was obtained by changing a fixed ion-repeller voltage of the scanning analyzer from shot to shot The shot-to-shot reproducibility of about 15% limited the signal-to-noise ratio. The ion axial energy E was obtained from the ion-repeller voltage V: $E = qV$.

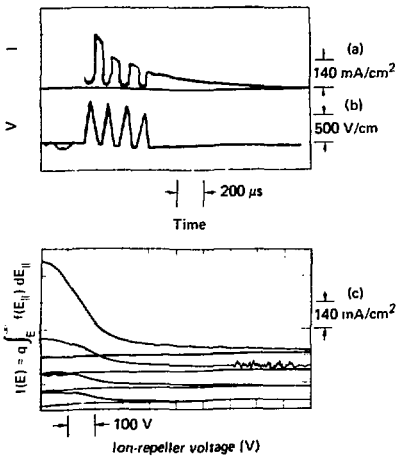

FIG. 14. The ion-repeller grid can be repetitively swept during one plasma pulse. In this example, taken during a 2XIIB run with the scanning analyzer, each sweep had a duration of 60 μs. The ion axial energy E was obtained from the ion repeller voltage V, $E = qV$. Shown are (a) the collector current vs time; (b) the ion repeller voltage vs time; and (c) the collector current vs ion-repeller voltage. Note that in (c) each subsequent sweep is displaced downwards.

sweeping the bias rapidly once or more during a shot (Fig. 14). The energy distributions are shown in integral form as measured; that is, we plot the measured ion current

$$I(E) = q \int_{E}^{\infty} f(E_{\parallel})\, dE_{\parallel} \quad , \tag{21}$$

versus $E = qV$ rather than plotting the differential form $f(E_{\parallel})$ versus $E_{\parallel}$. The latter is best obtained numerically, using data-smoothing techniques if necessary. The signal-to-noise ratio is limited to about 6 by shot-to-shot reproducibility (Fig. 13). Considerably higher signal-to-noise ratios are obtainable by sweeping in times short compared with the decay or growth times of the plasmas. The sweep rate of the ion-repeller grid in Fig. 14 is $dV/dt = 13 \times 10^6$ V/s. This limits the ion energy resolution to 5 eV at a 100-eV ion energy, as discussed in Sec. III.C.

IV. DISCUSSION OF ANALYZER DESIGN

The several topics discussed in this report on the design, construction, and operation of retarding-field gridded analyzers are not independent but must be considered as a set. A satisfactory design in general requires repeated iterations because design parameters may have contradictory requirements, so that initial requirements must be modified.

Accurate current measurements can be made as described in Sec. II. Measuring the energy distribution of the ions requires the additional design considerations described in Sec. III. In Sec. I, we discussed the designs of the scanning, 5-cm, and multicollector analyzers. The scanning analyzer provides the highest energy resolution because it is inserted into a uniform magnetic field (Sec. III.D). It is also large enough to confine higher-energy ion orbits. However, for a small loss of energy resolution, the 5-cm and multicollector analyzers are more conveniently located, simpler to build, easier to disassemble for maintenance or changes, more rugged mechanically, and designed to hold much higher voltage. The data presented demonstrate the performance of the scanning analyzer in measuring both ion-current and ion-energy distributions in the high electromagnetic noise environment of the 2XIIB experiment. The performance of the 5-cm analyzer in either 2XIIB or TMX was similar to that shown for the scanning analyzer.

ACKNOWLEDGMENTS

Productive conversations with W. F. Cummins, J. H. Foote, W. E. Nexsen, and J. E. Osher are gratefully acknowledged, along with the support and encouragement of F. H. Coensgen. Antony Stark helped with the rf ion source measurement. J. H. Williams and W. R. Call assisted with the mechanical design and were responsible for constructing the analyzers. C. K. McGregor and G. W. Leppelmeier suggested numerous clarifications that are incorporated in the text of this paper.

REFERENCES

1. F. H. Coensgen et al., Phys. Rev. Lett. 35, 1501 (1975).
2. D. E. Baldwin, H. L. Berk, and L. D. Pearlstein, Phys. Rev. Lett. 36, 1051 (1976).
3. F. H. Coensgen et al., Phys. Rev. Lett. 44, 1132 (1980); see also T. K. Fowler and B. G. Logan, Comments Plasma Phys. II, 167 (1977).
4. J. Arol Simpson, Rev. Sci. Instrum. 32, 1283 (1961).
5. Martin Caulton, RCA Rev. 26, 217 (1965).
6. Stavros Stephanakis and Willard H. Bennett, Rev. Sci. Instrum. 39, 1714 (1968).
7. Lyman Spitzer, Jr., Physics of Fully Ionized Gases, 2nd ed. (Interscience, New York, 1962), p. 22.
8. C. F. Barnett et al., "Atomic Data for Controlled Fusion Research," Rept. ORNL-5206 and 5207, 1977 (unpublished).
9. R. N. Sudan and R. V. Lovelace, Phys. Rev. Lett. 31, 1174 (1973).
10. B. G. Logan, et al., Phys. Rev. Lett. 37, 1468 (1976).
11. I. Langmuir and K. T. Compton, Rev. Mod. Phys. 3, 244 (1931).
12. W. C. Turner, A. W. Molvik, and J. Williams, The First Topical Conf. on Diag. of High Temp. Plasmas (Knoxville, Tenn., 1976) (unpublished).